Hindawi
Geofluids
Volume 2019, Article ID 3925462, 15 pages
https://doi.org/10.1155/2019/3925462

Research Article

Research on the Hydrochemistry and Fault Control Mechanism of Geothermal Water in Northwestern Zhangzhou Basin

Haonan Gan,[1,2] **Guiling Wang**,[2] **Xiao Wang**,[3] **Wenjing Lin**,[2] **and Gaofan Yue**[2]

[1]*State Key Laboratory for Mineral Deposits Research, School of Earth Sciences and Engineering, Nanjing University, 210093 Nanjing, China*
[2]*Institute of Hydrogeology and Environmental Geology, 050061 Shijiazhuang, China*
[3]*Hebei Geo University, 050031 Shijiazhuang, China*

Correspondence should be addressed to Guiling Wang; guilingw@yeah.net

Received 11 January 2019; Revised 28 May 2019; Accepted 26 June 2019; Published 14 August 2019

Guest Editor: Roman Makhnenko

Copyright © 2019 Haonan Gan et al. This is an open access article distributed under the Creative Commons Attribution License, which permits unrestricted use, distribution, and reproduction in any medium, provided the original work is properly cited.

The Zhangzhou Basin (ZB) is one of the most important hydrothermal regions in the southeast coast of China, with abundant underground thermal water resources. The hydrothermal region is located within widely scattered acid igneous rocks. Because of the low permeability of granitoids, the geothermal water flow is strongly controlled by fault structures. Previous studies mainly focused on the center of ZB and provided little understanding on the geochemistry and fault controlling mechanism of peripheral areas of the basin. In this study, the chemical compounds and elements of both thermal and cold underground waters of the Northwestern Zhangzhou Basin (NZB) were tested. Using cluster analysis, geochemical analysis, chemical geothermometers, silica vs. enthalpy mixing model, and structural interpretation of remote sensing, this study found that the thermal water in the research area mixes with shallow cold water in different proportions. The reservoir temperature ranges from 106°C to 147°C and differs between different sides of the Tianbao-Jinshan Fault (TJF) due to fault control. The difference in the circulation depth of underground thermal water causes this reservoir temperature disparity. The circulation depth of underground thermal water in research area ranges from 3.65 km to 5.44 km, which means the circulation depth of thermal water of the northwestern area is deeper than that of the central area of the basin.

1. Introduction

Fujian Province, which contains several thermal springs with relatively high temperature and large mass flow rates, is one of the most important geothermal activity zones in the eastern Chinese continent [1–5]. Scholars have conducted detailed analysis on the geological and hydrological conditions and the source, storage, and cover characteristics of the hydrothermal system of the Zhangzhou geothermal field during the 1980s and 1990s [6–12]. The Zhangzhou geothermal field is reported to be an underground convection system controlled by regional faults and heated by deep heat sources [4, 6–8]. Pang systematically discussed the distribution law of temperature in the center of the Zhangzhou Basin (ZB) and the characteristics of fault thermal control and calculated the reservoir temperature [6]. Han and Zhuan indicated that the ZB was formed by the obstruction of the NE-SW direction compressive torsional fault zone, which causes hot water to move up and out of the surface to form a hot spring, and the source of geothermal water in the ZB is meteoric precipitation [7]. Wang et al. believed that meteoric water transported underground to the central area of the ZB and reached 140°C at 3.5-4 km [8]. Nian suggested that the two faults in nearly the E-W direction and NE-SW direction are water-blocking faults while the NW-SE direction faults are water-guiding faults [11]. They together controlled the hydrothermal activity of the ZB. However, previous studies on the hydrothermal activities were limited to the interior of the ZB, and detailed studies on the hydrochemical characteristics of the underground geothermal water and cold water on the periphery of the ZB were not carried out.

This study assesses the relationship between thermal spring and cold water through cluster analysis (CA) and hydrochemical analysis of several hot springs (thermal wells)

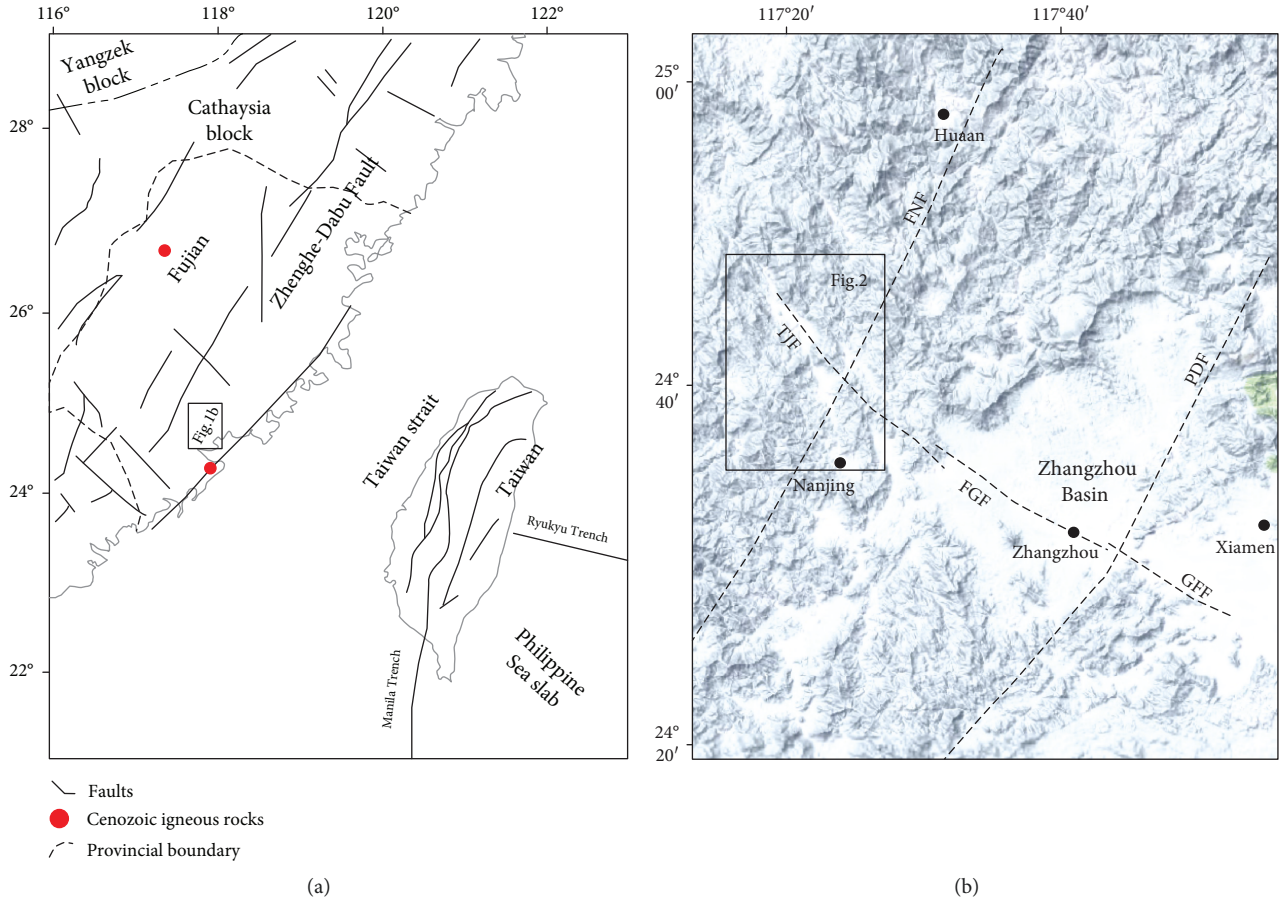

FIGURE 1: Tectonic location of the NZB (revised from [16]). FNF: Fuan-Nanjing Fault; TJF: Tianbao-Jinshan Fault; FGF: Fengle-Guanyinshan Fault; GFF: Guanyinshan-Fugong Fault.

and cold springs (wells) exposed in the Northwestern Zhangzhou Basin (NZB). This study offers new geochemical data for the NZB, and reservoir temperature corresponding to the geothermal water was calculated, and the control effect of the main faults on the underground thermal convection in the NZB was analyzed. This provides new evidence for thermal control of the fractures in the Zhangzhou area.

2. Geological Setting

The NZB is located in the southern part of Fujian Province, at the junction between the southeast Eurasian plate and the Philippine Sea plate. It is located in the coastal Pacific continental margin active belt of the Meso-Cenozoic and is known for its strong tectono-magmatism, which is a part of the Pacific Rim magmatic belt [13, 14]. The tectonic framework of Fujian Province is mainly divided into two tectonic units, i.e., the Huaxia block and the southeast coastal volcanic magmatic zone, which is divided by the Lishui-Zhenghe-Dapu Fault zone (Figure 1).

The collision and thrusting of the Philippine Sea plate with the Eurasian plate from the late Pliocene to the late Pleistocene and the recent expansion of the Taiwan strait have led to a strong neotectonic activity in the region [10, 15]. The NZB is a part of the middle and low temperature geothermal activity zone along the southeast coast of China.

The main geothermal anomaly area of the NZB is located in the late Yanshan granites. The main outcrops are quaternary sandy and eluvial sediments, late Mesozoic sedimentary rocks, and late Yanshan granites. Strata from Cretaceous to Pleistocene were missing in the study area, and the acidic granites of Jurassic to cretaceous were widely distributed (Figure 2).

Quaternary sediments mainly consist of sandy and eluvium deposits. Among these, the sandy deposits mainly consist of alluvium, alluvial, and marine deposits, which are generally 20–30 m thick. They are the marine-terrigenous facies of the late Pleistocene to the Holocene. The late Pleistocene (Qp_3l) residues mainly consist of a sandy gravel layer, which has good porosity and permeability. It is the main aquifer of geothermal water. The Holocene (Qhc) residues are mainly weathered acidic granites with a thickness of 10–30 m.

Mesozoic sedimentary rocks mainly consist of the Triassic and Jurassic sedimentary rocks and metamorphic rocks, distributed towards the southeast of the study area, with a thickness of 30-150 m. From bottom to top, the late Triassic Wenbinshan formation (T_3w), early Jurassic Lishan formation (J_1l), and middle Jurassic Zhangping formation (J_2z) are shown in sequence. The formation lithology of the Mesozoic is dominated by feldspathic quartz sandstone, siltstone, and hornstone.

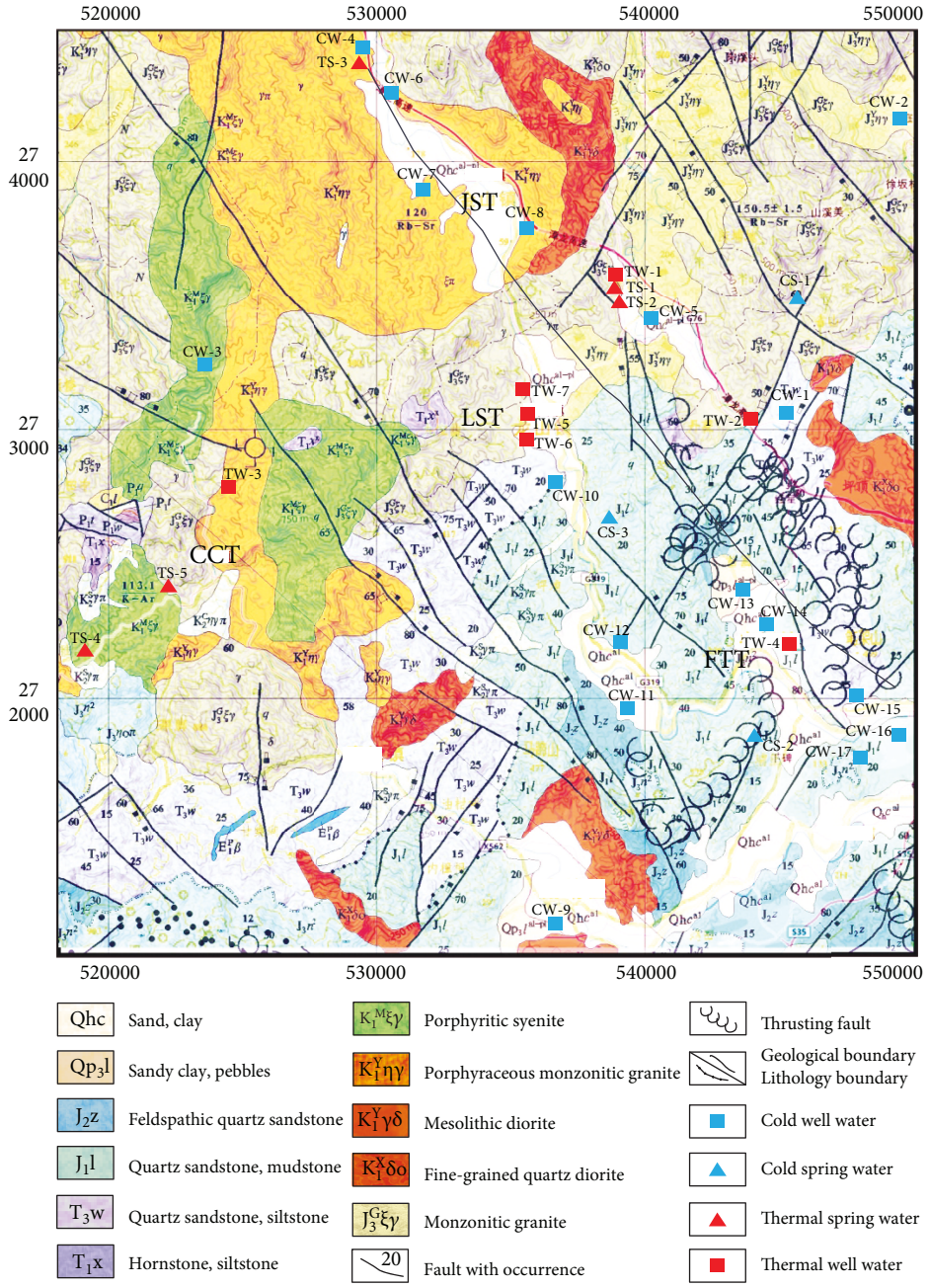

Figure 2: Geothermal and geological map for the NZB. JST: Jinshan Town; LST: Longshan Town; CCT: Chuanchang Town; FTT: Fengtian Town.

The acidic granites of late Yanshan in the study area mainly consist of Jurassic monzonitic granite ($J_3^{G}\xi\gamma$) and Cretaceous porphyritic syenite ($K_1^{M}\xi\gamma$), porphyraceous monzonitic granite ($K_1^{Y}\eta\gamma$), Mesolithic diorite ($K_1^{Y}\gamma\delta$), and fine-grained quartz diorite ($K_1^{X}\delta o$). The acidic granites are distributed widely, with a shallow burial depth and a large area exposed to the surface.

The thermal springs in the NZB are distributed in along the NE direction (Figure 2). According to previous studies, while most of the thermal springs are located at the rise or depression of the Curie depth in the deep, a few are located at the inflection point of the rise or depression of the Curie depth in the deep [17], which indicates that the shallow surface geothermal anomaly is closely related to the thermal background at depth. Pang believes that the Zhangzhou geothermal system forms a high permeability zone through the intersection of regional faults [6]. The formation of thermal springs in the groundwater discharge area indicates that other neotectonic strike faults, except the regional faults in the NE direction, also play a key role in the formation and distribution of thermal springs.

3. Materials and Methods

Sampling of water from the fluid discharges was performed in December 2016. Sampling locations are shown in

Figure 2. A total of 36 water samples were collected, including 7 from geothermal wells, 5 from thermal springs, and 24 cold water samples. Water parameters including temperature, pH, EC, and total dissolved solids (TDS) were measured in situ using a portable multipara meter (HQ40D, Hach), which was calibrated using a standard solution before use. For SiO_2 analyses, the geothermal water samples were diluted to 10% of their initial concentration with deionized water. For metallic and cation element analyses, samples were acidified with HNO_3 to pH 1. No reagents were added to the samples for inorganic anion analysis. All water samples were analyzed in the Key Laboratory of Groundwater Science and Engineering of the Ministry of Land and Resources.

The concentrations of major cations and trace elements were detected by ICP-AES (ICAP6300, Thermo Fisher Scientific) and ICP-MS (7500C, Agilent), respectively. Anions were determined using Ion Chromatography (DX-120, Thermo Fisher Scientific). Table 1 summarizes the precision and accuracy errors (in %) reported for the chemical analyses, including the limits of detection (LODs), for each one of the elements. Accuracy was evaluated by analyzing water-certified standards as external testers [18]. The ion charge imbalances for the water samples were calculated using the program AquaChem, and the results showed that all of the geothermal water samples have a charge imbalance less than ±3%, while most of the cold water samples have a charge imbalance more than ±10%, as the concentration is too low which leads to a larger error in the detection.

Table 1: Precision, accuracy, and detection limits for the elemental chemical analyses.

Chemical elements	Precision (%)	Accuracy (%)	LOD
Li^+	9	5.9	0.001
Na^+	5	9.5	0.005
K^+	1	10	0.03
Mg^{2+}	2.2	1.6	0.002
Ca^{2+}	2.3	5.9	0.7
F^-	8.3	-1.6	0.01
Cl^-	1.3	0.4	0.03
NO^{2-}	2.6	3.6	0.01
NO^{3-}	0.9	-0.7	0.01
SO_4^{2-}	1	1.6	0.03
PO_4^{3-}	2.1	5.5	0.02
HCO_3^-	3	3	1
Si	1.6	10.5	200
Sr	1.8	3.4	0.04

LOD: limit of detection (estimated according to the statistical methodology suggested by IUPAC [19]; major elements (mg/kg); trace elements (μg/kg)).

4. Results

CA is a convenient and effective means for exploring geochemical patterns and interpreting hydrochemical characteristics [20]. Cluster analysis was used as an analysis of variance approach (hierarchical cluster) to measure a distance between variable clusters, attempting to minimize the sum of squares of any two clusters that could be formed at each step (square Euclidean distance). Hydrochemical data with similar properties were clustered in a group [21]. In this study, the major elements, including K, Na, Ca, Mg, Cl, SO_4, and HCO_3, were considered while evaluating the characteristics of the geothermal spring samples using the average linkage hierarchical method, which is designed to optimize the minimum variance within groups (Figure 3). To avoid misclassifications arising from the different order of magnitude of the variables, the variances for each variable were standardized [22, 23].

The hydrochemical characteristics of all water samples are summarized in Table 2. The hydrochemical data used to support the findings of this study are included within the article. The samples were divided into two groups, G1 and G2, and G1 was further divided into two subgroups, i.e., G1-1 and G1-2. All the geothermal water samples were clustered in the G1-2 subgroup. Cold water samples were clustered in G1-1 and G2, where the cold well samples were not significantly different from the cold spring samples. G2 only contained three cold water samples. It can be seen from Table 2 that the concentration of major elements of G2 is significantly higher. This indicates that while the content of K^+, Na^+, and Ca^{2+} in G2 is much higher than that of other samples, the content of Cl^-, SO_4^{2-}, and HCO^{3-} in G2 is also higher than that of cold water samples of G1-1.

It can be seen from the sampling locations (Figure 2) that the samples of each group do not have a good spatial aggregation and are distributed throughout the study area. However, the G1-2 subgroup (geothermal water group) is mainly located in the canyon along the Tianbao-Jinshan Fault (TJF), followed by the area around Chuanchang Town (CCT). The G2 group is mainly located in the southeastern part of the study area, in the quaternary canyon along the E-W or N-W direction.

5. Discussion

5.1. Hydrogeochemical Characteristics. The temperature of the water samples belonging to the low temperature geothermal water ranged from 42.1 to 65°C in the study area, with a pH of 7.7-9.17. The temperature of cold water samples ranged from 20.8-27.2°C, with a pH of 5.37-7.31, which is less than that of the geothermal water (Table 2). According to the piper triangle plot (Figure 4), there are hydrochemical differences between the geothermal water and cold water samples. All the geothermal water samples contained Na^+ as the predominant cation and had more SO_4^{2-} than cold water samples. Most samples of geothermal water contain HCO^{3-} and SO_4^{2-} as the predominant and subordinate anions. The cold water samples, though a part of two subgroups, were relatively dispersed and did not show aggregation and were of HCO_3-Ca·Na and SO_4-Ca·Na types.

The relative contents of Ca^{2+} and HCO_3^- in the G1-1 subgroup were found to be significantly higher. Compared with those of the G1-2 subgroup, the cations of the G2 group were similar, while anions showed relatively high Cl^- and SO_4^{2-} and low HCO_3^-.

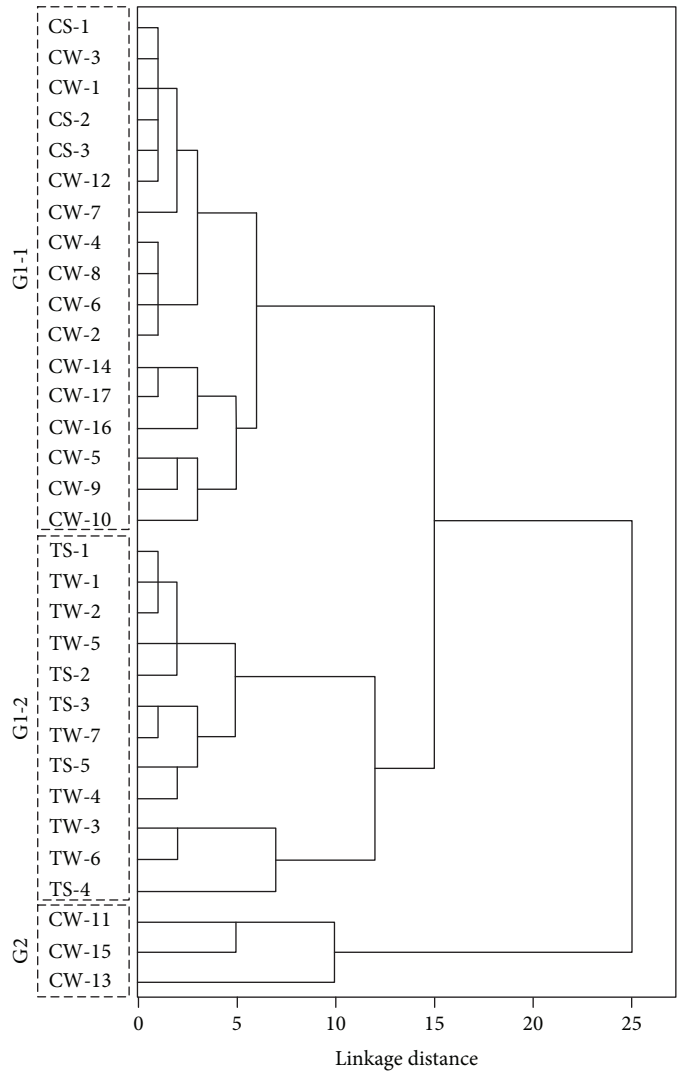

Figure 3: Cluster analysis of water samples of the NZB.

The geothermal water of the central area of the ZB is of Cl-Na·Ca type, where the Cl^- composition mainly occurs due to mixing with seawater [6]. The low concentration of Cl^- in geothermal water samples from the study area indicates that the NZB is not affected by the mixing of seawater. Additionally, the geothermal water samples (G1-2) show a clear linear relation in the Cl-SO_4-HCO_3 triangle diagram and the Na-K-Mg triangle diagram, indicating that geothermal fluids are generally mixed with shallow cold water.

5.2. Reservoir Temperature

5.2.1. Geothermometric Applications. Chemical geothermometers, including a silica geothermometer (the solubility of silica changes as a function of temperature and pressure) and a cation geothermometer (the equilibrium constants for exchange and alteration reactions are temperature dependent), were applied to estimate the temperatures of the geothermal reservoirs. The cation geothermometer requires geothermal fluids to achieve water rock balance and avoid the mixing of ion-rich fluids such as seawater. For the center of the ZB, Na, K, Mg, etc., in geothermal water are not controlled by temperature due to the large amount of seawater mixing, which reduces the applicability of the cation geothermometer. The Cl^- concentration of geothermal water in the NZB indicates that there is no mixing with seawater. Hence, only the equilibrium state of geothermal water with rock could be identified. Figure 5 shows that all cold samples fall in the field of the immature water area, and all geothermal water samples fall in the field of partially equilibrated or mixed waters, suggesting that geothermal waters from this area have generally reached partial fluid-rock chemical equilibrium. Therefore, a cation geothermometer and a silica geothermometer were used to determine the equilibrium situation of geothermal water and calculate the reservoir temperature. Figure 5 shows a linear relationship between the geothermal water samples, indicating that mixing of cold water occurs during the rise of geothermal water. Therefore, the silica-enthalpy mixing model was also used in this study. This model can examine the reservoir temperatures of deep geothermal water and mixed shallow geothermal water [24]. Enthalpy is used as

Table 2: Chemical analysis result of water sample of the NZB (in mg/L, except for pH in standard pH units and T in ˚C).

Group	Sample ID	Sample type	T	pH	K	Na	Ca	Mg	Cl	SO_4	HCO_3	CO_3	Li	F	SiO_2	Sr
G1-1	CS-1	Cold spring	21.8	6.75	1.82	3.88	2.33	0.18	1.75	1.83	27.51	0	<0.005	0.17	19.21	0.007
	CS-2	Cold spring	23.7	6	0.29	0.78	0.61	0.22	1.75	3.1	9.17	0	<0.005	0.11	7.25	0.004
	CS-3	Cold spring	23.2	5.89	1.65	1.86	1.1	0.28	2.8	2.57	9.17	0	<0.005	0.14	13.96	0.008
	CW-1	Cold well	26.9	5.94	1.51	1.76	3.2	0.71	1.75	1.86	17.12	0	<0.005	0.13	14.16	0.021
	CW-2	Cold well	23.3	6.72	2.27	9.65	13.81	1.63	2.45	1.06	67.25	0	<0.005	0.25	52.17	0.114
	CW-3	Cold well	23	6.34	2.34	2.98	2.97	0.22	1.75	1.16	24.46	0	<0.005	0.18	23.15	0.004
	CW-4	Cold well	20.8	6.65	2.33	4.32	9.31	1.21	1.75	3.59	42.8	0	<0.005	0.2	19.63	0.063
	CW-5	Cold well	25.1	6.93	3.08	27.97	18.37	0.94	8.75	10.98	100.9	0	0.035	2.4	48.11	0.081
	CW-6	Cold well	23.3	6.33	2.94	6.37	7.8	1.4	3.5	2.05	24.46	0	<0.005	0.17	28.35	0.095
	CW-7	Cold well	24	5.86	5.21	2.94	5.98	0.58	9.1	0.9	6.11	0	<0.005	<0.10	6.08	0.038
	CW-8	Cold well	27.2	6.54	2.3	9	11.46	1.46	1.75	4.82	55.03	0	<0.005	0.22	50.41	0.077
	CW-9	Cold well	22.8	6.68	2.77	12.89	16.54	2.36	11.9	1.24	91.71	0	<0.005	0.32	46.23	0.231
	CW-10	Cold well	24.8	7.31	6.29	2.02	19.13	0.34	1.75	8.73	67.25	0	<0.005	0.2	15.19	0.495
	CW-12	Cold well	22.6	5.92	1	2.13	0.91	0.39	4.9	1.4	12.23	0	<0.005	0.13	14.82	0.012
	CW-14	Cold well	23.5	5.73	6.48	3.4	11.8	2.17	12.95	14.09	12.23	0	<0.005	0.25	12.22	0.058
	CW-16	Cold well	23.6	5.37	6.64	18.04	10.29	0.72	19.26	0.96	6.11	0	<0.005	0.18	7.55	0.048
	CW-17	Cold well	24.2	6.12	3.85	8.95	12.6	2.67	15.76	4.38	48.91	0	<0.005	0.15	20.54	0.104
G2	CW-11	Cold well	24.7	6.47	26.37	13	16.8	5.11	15.76	32.76	42.8	0	<0.005	0.14	11.75	0.086
	CW-13	Cold well	25.1	6.18	21.27	20.01	12.63	2.53	33.26	12.71	33.63	0	<0.005	0.22	20.59	0.148
	CW-15	Cold well	23.2	6.58	15.74	8.14	23.9	3.79	12.25	26.13	48.91	0	<0.005	0.2	16.07	0.165
G1-2	TS-1	Thermal spring	53	8.82	1.35	70.69	2.84	0.04	7	36.42	70.31	21.05	0.06	11.68	67.26	0.088
	TS-2	Thermal spring	45.5	8.9	1.11	68.62	2.97	0.05	7	35.9	48.91	30.07	0.06	11.12	68.82	0.081
	TS-3	Thermal spring	45	8.79	1.64	81.8	6.14	<0.013	12.25	55.61	94.77	12.03	0.07	10.1	60.59	0.14
	TS-4	Thermal spring	50.1	7.7	3.6	116.4	10.85	0.22	14.71	53.89	229.3	0	0.17	13.58	81.92	0.227
	TS-5	Thermal spring	60.2	8.57	2.55	109.2	11.17	0.19	15.06	106.2	116.2	12.03	0.02	11.24	69.23	0.259
	TW-1	Thermal well	42.1	8.85	1.26	69.98	2.87	0.03	8.75	36.44	58.08	24.05	0.06	11.47	69.18	0.079
	TW-2	Thermal well	48.4	8.8	1.31	71.71	3.46	0.05	10.5	40.85	67.25	18.04	0.05	12.32	57.81	0.096
	TW-3	Thermal well	55.8	8.4	2.51	127	12.46	0.14	22.76	135.9	137.6	6.01	0.17	11.01	65.20	0.656
	TW-4	Thermal well	50.2	8.67	2.55	98.27	6.88	0.05	9.1	83.36	116.8	9.02	0.08	13.67	76.10	0.127
	TW-5	Thermal well	50	9.17	1.38	86.36	3.48	<0.013	15.41	52.69	67.25	18.04	0.07	12.11	62.29	0.161
	TW-6	Thermal well	65	8.45	2.08	116.2	9.25	0.07	24.51	100.4	137.6	3.01	0.12	11.75	57.16	0.389
	TW-7	Thermal well	60	8.6	1.11	74.91	3.6	0.07	12.25	47.63	88.65	7.22	0.04	11.66	46.92	0.077

a coordinate rather than temperature in these models, since the combined heat contents of two samples at different temperatures are conserved when they are mixed, but the combined temperatures are not [25, 26].

Since the temperature-dependent solubility of silica as a geothermometer method has been proposed [27, 28], subsequent studies have delimited the temperature limits according to the different solubilities of the silica polymorphs such as quartz, chalcedony, and amorphous silica [29–33]. Among these, the amorphous silica geothermometer is employed for temperatures below 100˚C [34]. Since the solubility of quartz appears to control the dissolved silica in a geothermal reservoir at temperatures higher than 120˚C-180˚C [35], which is the case in the investigated geothermal area [6], the quartz geothermometer was adopted in this study. The temperatures measured by the quartz geothermometer between the values of maximum steam loss and no steam loss were chosen [35]. In this study, the reservoir temperature values measured using the quartz geothermometer were selected for the optimum temperature of samples, taking into account the measured emerging temperature and the mass flow rate of the corresponding spring [29]. Since the values of the emerging temperatures in the study area are lower than the local boiling point, the quartz geothermometer without steam loss was used for measuring reservoir temperature.

Among the cation geothermometers based on exchange reaction, Na/K and K/Mg geothermometers were used in this study. The Na/K geothermometer was used as the Na/K ratio is independent of spring water evaporation [36, 37]. The Na/K geothermometer is suitable for conditions above 100˚C, especially for cases when the temperature is higher than 180˚C, as it is used in fluid-rock chemical equilibrium [38]. The Na/K geothermometer was chosen as the K/Mg ratio records intermediate temperatures between the reservoir values and the outlet values as it reequilibrates immediately upon mixing with colder water [39, 40]. Thus, it can be

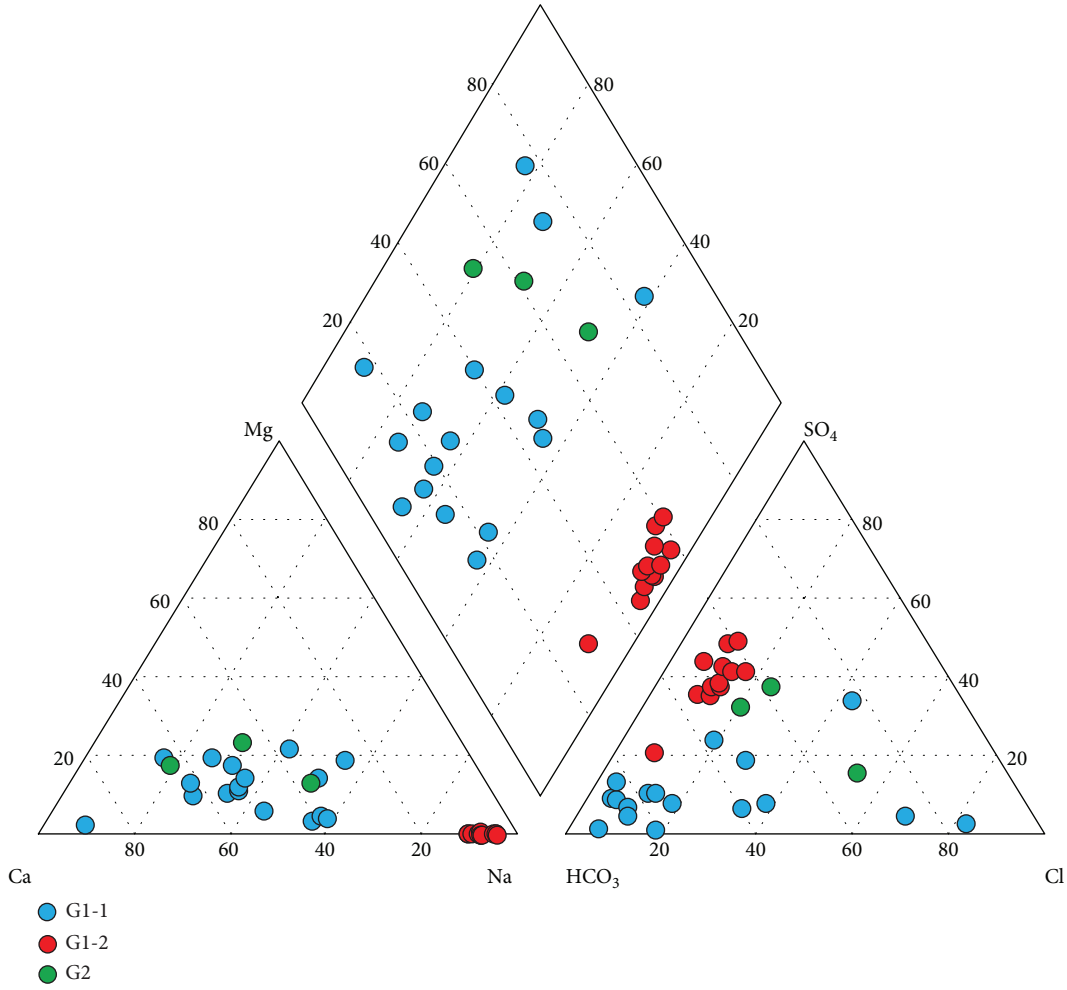

Figure 4: Piper diagram of underground water samples in the research area.

used complementarily with Na/K to reflect reservoir characteristics. The formulas of chemical geothermometers and estimated results are listed in Tables 3 and 4.

5.2.2. Quartz and Cation Geothermometers. The geothermometers show significantly different values of the reservoir temperature of the NZB (Table 4). The reservoir temperatures calculated by the quartz and Na/K geothermometer [36] are similar, both lower than the values of the Na/K geothermometer [43] and the silica-enthalpy mixing model. The K/Mg geothermometer yielded a lower reservoir temperature than other geothermometers.

The quartz geothermometer [41] yielded a reservoir temperature of 98-126°C, mainly of 117°C. This relatively low reservoir temperature could be due to several reasons. Firstly, a SiO_2 geothermometer is suitable for the temperature range of 150-225°C, and temperatures under 150°C may cause error as the presence of SiO_2 minerals other than quartz would control the SiO_2 concentration. Secondly, dilution due to mixing could decrease the absolute quartz concentration and in turn produce incorrect lower reservoir temperatures [26, 44]. Thirdly, steam loss of deep thermal fluids before mixing with cold water may have an influence on the SiO_2 concentration. Fourthly, the pH of a fluid is a key parameter controlling SiO_2 solubility and is very sensitive to SiO_2 temperature, especially for pH values in excess of 8 [39, 40]. According to the calculation of Nitschke et al. [45], for the same SiO_2 concentration, the temperature measured by an SiO_2 geothermometer at pH 9 is lower than the temperature measured at pH 8.5 by 5-20°C. The SiO_2 geothermometer [42] yielded a reservoir temperature of 98-128°C, which is close to the result of the quartz geothermometer [41].

The reservoir temperature of 94-133°C, as calculated by the Na/K geothermometer [43], is relatively lower as compared to other Na/K geothermometers. A possible reason for this could be that the Na/K geothermometer is suitable for temperatures higher than 180°C [46]. Thus, in a geothermal field with relatively low temperatures, like the study area, the calculated temperature of the Na/K geothermometer is lower due to the influence of cold water dilution and steam loss before the mixing. Secondly, high Ca^{2+} concentrations may have an influence on the Na/K equilibrium. The Na/K geothermometer [44] yielded a reservoir temperature of 115-153°C, mainly of 122°C, which is higher than that of Fournier [43], and close to the result of the silica-enthalpy mixing model. The Na/K geothermometer [42] yielded a reservoir temperature of 61-190°C, with a relatively large range for each sample. This geothermometer [42] is

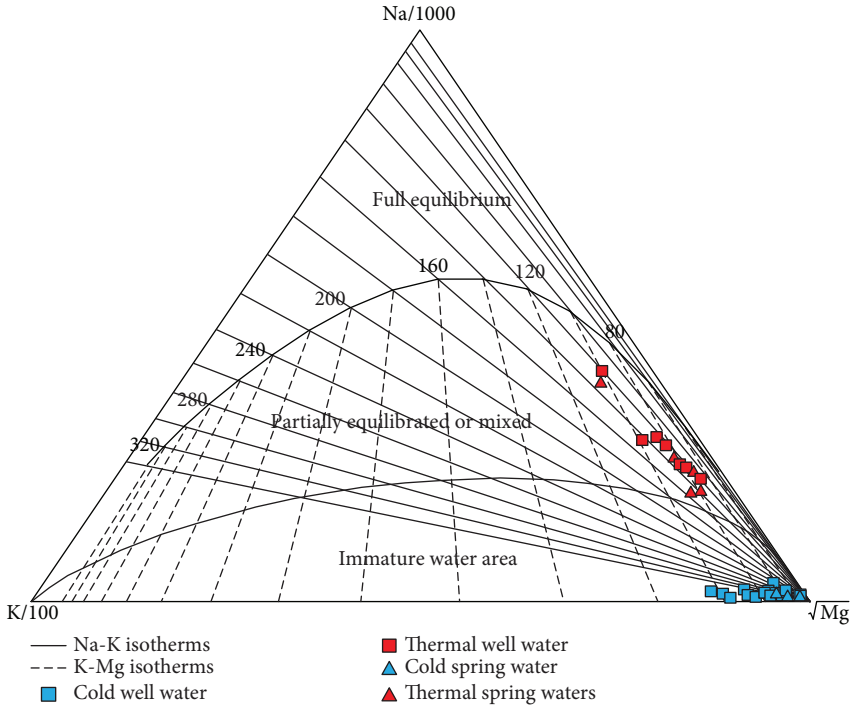

Figure 5: Na-K-Mg diagram for geothermal water samples in the research area.

Table 3: Formulas of chemical geothermometers used in this study.

Geothermometer	Formula	Reference
Quartz	$t = \frac{1309}{5.19 - \log \mathrm{SiO_2}} - 273.15$	Fournier [41]
	$t = -\{44.119(\pm 0.438)\} + \{0.24469(\pm 0.00573)\}S - \{1.7414 \times 10 - 4\,(\pm 1.365 \times 10 - 5)\}S2 + \{79.305(\pm 0.427)\} \log S*$	Verma and Santoyo [42]
Na/K	$t = \frac{1217}{\log (\mathrm{Na/K}) + 1.483} - 273.15$	Fournier [43]
	$t = \frac{1390}{\log (\mathrm{Na/K}) + 1.750} - 273.15$	Giggenbach [44]
	$t = \frac{1289 \pm 76}{\log (\mathrm{Na/K}) + 1.615(\pm 0.179)} - 273.15$	Verma and Santoyo [42]
K/Mg	$t = \frac{4410}{13.95 - \log (\mathrm{K^2/Mg})} - 273.15$	Giggenbach [44]

*Applicable for 20–210°C, S is the concentration of SiO_2.

supposed to offer the upper and lower temperature limits calculated by the Na/K geothermometer since results of the other two Na/K geothermometers [43, 44] fell into the range of 61-190°C.

The reservoir temperature calculated by the K/Mg geothermometer is in between the values provided by other geothermometers. The possible reasons could be that mixing of deep geothermal water with cold water having a high Mg^{2+} concentration caused changes in K^+ and Mg^{2+} concentrations and the deviation of reservoir temperatures.

5.2.3. Silica-Enthalpy Mixing Model. The silica-enthalpy mixing model was applied in this study to estimate the temperatures of the geothermal reservoir and identify the mixing processes [38, 47–49]. The samples were required to have no heat loss after mixing, and superheated water and boiling water are not suitable for the silica-enthalpy mixing model. The silica-enthalpy mixing model was suitable for this study as the emerging temperatures were all lower than the boiling point (Tables 2 and 4). In the silica-enthalpy model, the silica concentrations of the analyzed samples are plotted against

Table 4: Results of reservoir temperature of geothermal water samples in the study area (temperature in °C and concentration in mg/L).

Sample ID	Emerging temperature	SiO_2	Quartz (no loss of steam)	Quartz (Verma and Santoyo)	Na/K (Fournier)	Na/K (Giggenbach)	Na/K (Verma and Santoyo)	K/Mg	Silica-enthalpy mixing model (C1)	Silica-enthalpy mixing model (C2)
TS-1	53	67.26	116.17	114.84-118.17	106.92	127.54	72.14-159.49	85.64	156.14	126
TS-2	45.5	68.82	117.33	115.96-119.32	98.55	119.38	65.19-149.83	78.01	198.93	142
TS-3	45	60.59	110.99	109.83-113.02	109.44	129.99	74.22-162.41	105.90	170.64	132
TS-4	50.1	81.92	126.35	124.68-128.32	133.51	153.28	94.02-190.25	88.92	221.98	148
TS-5	60.2	69.23	117.63	116.25-119.62	117.58	137.89	80.94-171.81	82.05	156.61	126
TW-1	42.1	69.18	117.59	116.21-119.58	103.91	124.61	69.64-156.01	87.55	207.48	144
TW-2	48.4	57.81	108.70	107.61-110.75	104.65	125.32	70.25-156.86	82.08	150.19	123
TW-3	55.8	65.20	114.62	113.33-116.62	108.70	129.27	73.61-161.55	85.48	152.81	125
TW-4	50.2	76.10	122.48	120.94-124.45	123.41	143.53	85.74-178.56	99.45	178.48	136
TW-5	50	62.29	112.35	111.14-114.37	97.95	118.79	64.69-149.13	101.08	152.33	125
TW-6	65	57.16	108.16	107.09-110.21	103.61	124.32	69.39-155.67	89.55	116.44	108
TW-7	60	46.92	98.87	98.08-100.98	94.28	115.20	61.64-144.89	73.97	110.73	106

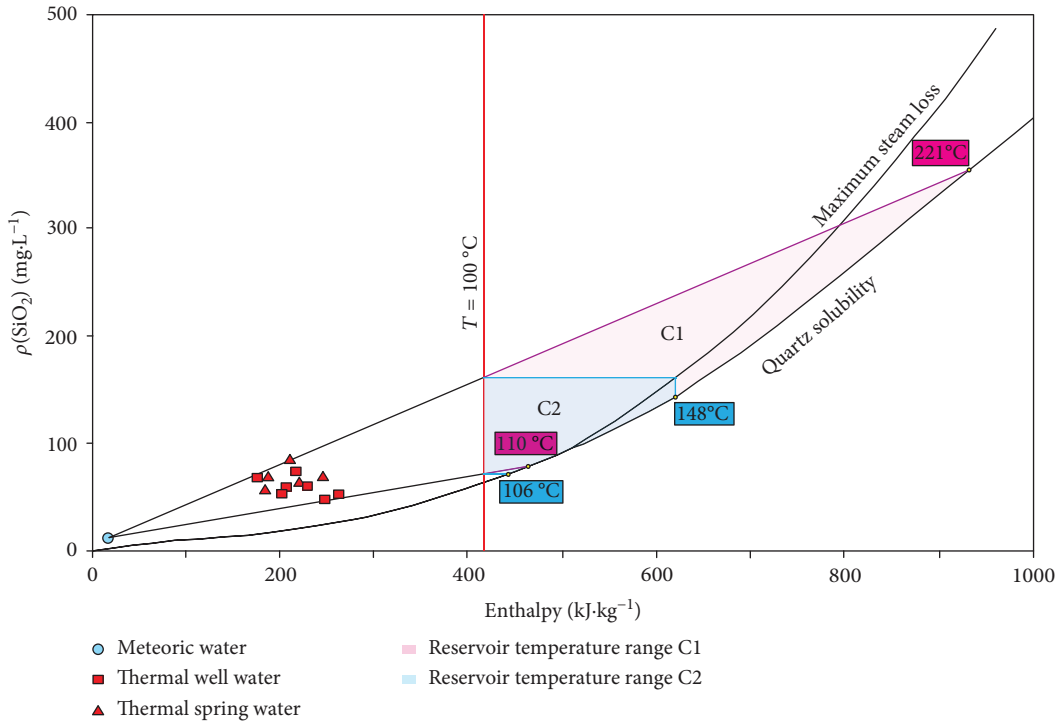

Figure 6: Silica vs. enthalpy mixing models of geothermal water samples in the research area.

their corresponding on-site enthalpies (Figure 6). The enthalpy values are determined using international steam tables [50].

For application to emerging geothermal samples, two end-member fluids were considered: a cold groundwater sample and an initial deep geothermal water sample. Figure 6 shows that the extension lines that connect all geothermal water samples with cold water points have intersections with the quartz solubility curve, which indicates that all geothermal water samples in the study area mix with cold water during the cooling process. The point of the initial deep geothermal water can be obtained using two different methods. For the scenario in which no steam is lost before mixing, one method plots the silica and heat contents (enthalpies) of the cold and emerging spring waters as two points and then draws a straight line through these points to intersect the quartz solubility curve; the intersection range C1 then provides the original silica contents and enthalpies of the deep geothermal water. The corresponding temperatures of the geothermal reservoir were 110-221°C, mainly of 155°C. For the scenario in which the maximum amount of steam is lost from geothermal water before mixing, the method plots the silica and heat contents of the cold and emerging spring waters as two points, draws a straight line through the points, and extends that line to intersect the vertical line from the enthalpy values of 419 J/g (corresponding to 100°C, the boiling point of water) and subsequently from this intersection point moves horizontally to the maximum steam loss curve and then moves vertically to intersect the quartz solubility curve. The original silica contents and enthalpies of the deep geothermal water components are provided by range C2. The corresponding temperatures of the geothermal reservoir are 106-148°C, mainly of 128°C.

5.2.4. Selected Reservoir Temperatures. Low temperature in the K/Mg geothermometer indicates a faster equilibration of K/Mg and mixing with Mg-rich shallow waters. The Na/K geothermometer shows the highest temperature when it approaches a mineral-fluid equilibrium. While the calculated reservoir temperature of Na/K is not high enough for approaching equilibrium, the reservoir temperature ought to be less than 150°C. According to the reservoir temperature calculated by the silica-enthalpy mixing model (C1, C2), if C1 represents the actual reservoir temperature of the NZB, then the Na/K geothermometer would have kept this temperature range, which is not in conformity with the calculation of Na/K. Additionally, the Na-K-Mg diagram indicated a temperature range of 120-160°C for geothermal water, mainly of 130°C. Therefore, C2 represents a reasonable reservoir temperature range. Thus, the reservoir temperature of the NZB ranges between 106 and 148°C, and steam loss occurs before mixing of the deep geothermal water with cold water.

The intersection range of C2 shows that the SiO_2 concentration of initial geothermal water is approximately 75-155 mg/L. In other words, the initial geothermal water with a reservoir temperature of 106-148°C would have an SiO_2 concentration of approximately 75-155 mg/L. Compared with the SiO_2-measured concentration of 48-72 mg/L in the NZB (Table 2), the difference could be explained by SiO_2 reprecipitation in partly equilibrated geothermal water. Moreover, it could be estimated that approximately 37-47% of the SiO_2 reprecipitates.

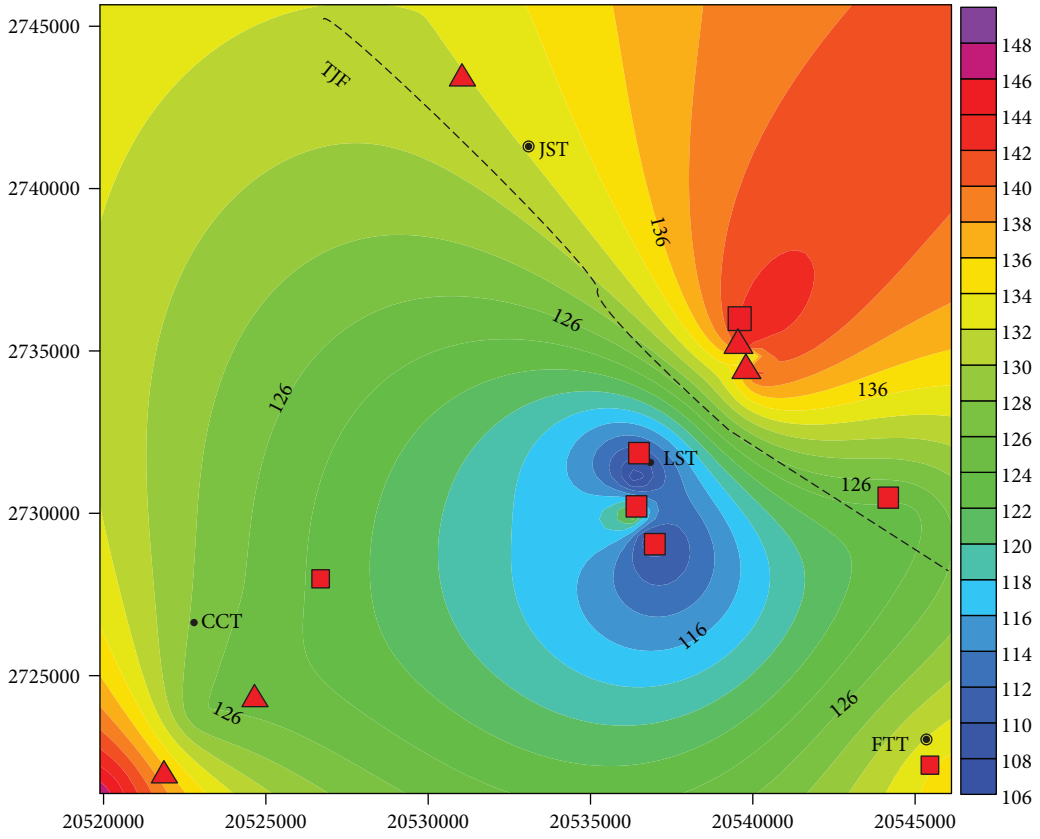

Figure 7: Contour map reservoir temperatures determined in "selected reservoir temperatures" of the study area (red square and triangle refer to thermal well water and thermal spring water. For abbreviations, see Figure 2).

5.3. Fault Control Mechanism Analysis. Contour maps were used to measure temperatures of the geothermal reservoirs (Figure 7). It can be seen that the reservoir temperature in the center of the NZB is generally low, and the areas with high thermal reservoir temperature are mainly in the north east and south west of the NZB. It should be pointed out that samples TW-6 and TW-7, which have higher emerging temperatures, have relatively lower reservoir temperature (Table 4). According to the silica-enthalpy mixing model, the mixing proportion of cold water of these samples is small. This may be explained by the fact that the initial fluid does not mix with a large amount of cold water when ascending to the surface. Hence, the emerging temperature is not significantly reduced.

Along the TJF, the reservoir temperature shows change on both sides, which indicates a regional fault control (Figures 1 and 7). According to Zhu et al. [17], the Fengle-Guanyinshan Fault (FGF) and the Guanyinshan-Fugong Fault (GFF) in the southeast of the study area are N-W trend tensional or tension-shear faults (Figure 8). The TJF, which is also a tension or tension-shear fault, is likely to be an extension of FGF and GFF in the N-W direction (Figure 8). It can also be seen from the structure interpretation map that the study area is the extension of the ZB along the northwest direction, which is consistent with the conclusion (Figure 8). The change in reservoir temperature on both sides of the TJF seems to indicate that the TJF has the thermal resistance effect. However, it is difficult for the TJF to block heat transfer as it is a tension or tension-shear fault.

Oxygen and hydrogen isotope data indicate that the source of geothermal water in the ZB is meteoric precipitation [7, 51]. Magmatic activities in the study area generally occurred during the Mesozoic era, which excludes the possibility of magmatic activities providing a heat source for geothermal water in the study area. Moreover, the thermal spring distribution in the NZB is strictly controlled by the fault structure, which provides a proper channel for the deep circulation of groundwater. Therefore, the heat of deep geothermal water of the NZB is mainly obtained by deep circulation through geothermal heating. Based on the above speculation, we suggest that since the TJF is located in the N-W canyon, the source of recharge is the meteoric water from mountains on both sides of the canyon. Due to the tension or tension-shear stress property of the TJF, the geothermal water emerges to the surface after circulation heating along the TJF. However, due to the difference in the depth of the circulating geothermal water on both sides (the depth of the fault is less, or the dip angle of the fault is small), the circulation of geothermal water on the NE side is deeper than that on the SW side. Therefore, though both sides flow to the surface along the TJF, different circulation depths lead to different reservoir temperatures, which leads to different reservoir temperatures on both sides of the TJF (Figure 9).

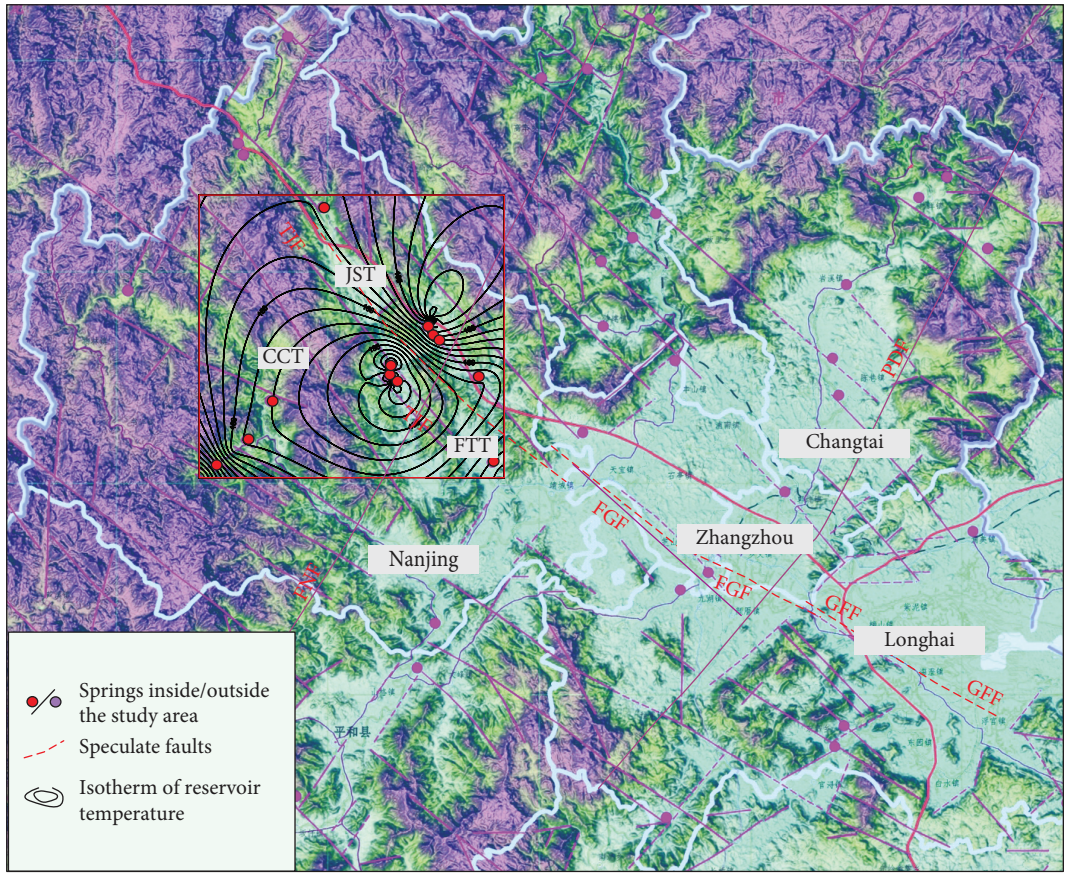

Figure 8: Map of the structural interpretation of remote sensing. The red square refers to the area of Figure 7. For abbreviations, see Figures 1 and 2.

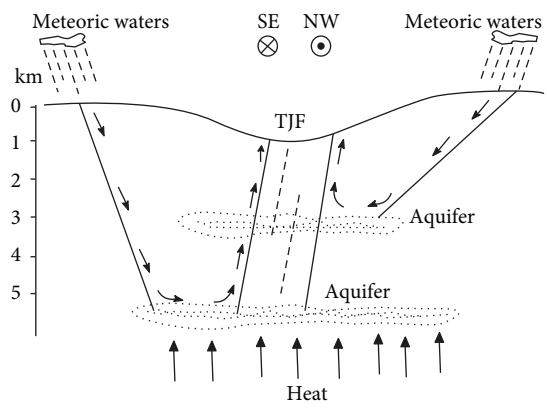

Figure 9: Simplified conceptual model of fault control mechanism of the NZB.

5.4. Circulation Depth of Geothermal Water. The deep geothermal water of the ZB mainly obtains its heat through geothermal heating due to deep circulation [6]. According to the investigation report of Minnan Geological Survey Team [52], the circulation depth of geothermal water in the ZB is about 3000 m. Xiong et al. calculated the circulation depth of 3.5-4.0 km based on results from the SiO_2 geothermometer [53, 54].

With the hypothesis that the geothermal water acquires heat through a certain circulation depth and increases its own temperature, which then ascends to the surface, the circulation depth of geothermal water can be estimated by

$$H = \frac{(T_{cal} - T_0)}{q + H_0}, \quad (1)$$

where H is the circulation depth in m, q is the geothermal gradient in ˚C/km, T_{cal} is the reservoir temperature of geothermal water in ˚C, T_0 is the mean annual air temperature of the NZB in ˚C, and H_0 is the soil depth of constant temperature in m.

According to the investigation report of Minnan Geological Survey Team [52], T_0 is taken as 21˚C and H_0 is taken as 30 m. The reservoir temperature is estimated using the calculation result of the silica-enthalpy mixing model. It is not easy to determine the value of q. In this study, the linear relation of temperature vs. depth in the deep well (HDR-1) in the ZB is used to calculate the geothermal gradient. The drilling depth is 4000 m. The lithology for 0-36 m is quaternary residual soil and for 37-4000 m is granitoid. Stable conductive temperature curve interval is taken to obtain the average geothermal gradient. According to the well logging of HDR-1, the linear relation of temperature vs. depth remains straight during the

Table 5: Calculation results for circulation depth of geothermal water in the study area (temperature in ˚C and depth in km).

Sample ID	Emerging temperature	Reservoir temperature (C2)	T_{cal} -T_0	Circulation depth
TS-1	53	126	105	4.50
TS-2	45.5	142	121	5.19
TS-3	45	132	111	4.76
TS-4	50.1	148	127	5.44
TS-5	60.2	126	105	4.50
TW-1	42.1	144	123	5.27
TW-2	48.4	123	102	4.38
TW-3	55.8	125	104	4.46
TW-4	50.2	136	115	4.93
TW-5	50	125	104	4.46
TW-6	65	108	87	3.74
TW-7	60	106	85	3.65

depth of 2000-3000 m; therefore, the average geothermal gradient of a relatively stable formation interval (2000-3000 m) is 23.47˚C/km; i.e., q is taken as 23.47˚C/km [55]. All the parameters were put in equation (1), and the circulation depth of geothermal water of the NZB range was calculated to be 3.65–5.44 km, mainly of 4.5 km, which is relatively deeper than the center of the ZB (Table 5) [51]. According to the calculation, the circulation depth on the NE side of the TJF is deeper than 4.5 km, and that on the SW side is less than 4.46 km.

6. Conclusion

All samples were divided into two groups (group 1 was further divided into two subgroups) using cluster analysis of major elements. All geothermal water samples were placed into one subgroup. The geothermal water was of Na-HCO_3·SO_4 type while the cold water was of Ca-Na-HCO_3 type. The low concentration of Cl^- in the geothermal water of the study area indicates that the NZB is not affected by mixing of seawater.

The reservoir temperature calculated by the silica-enthalpy mixing model (C1, C2) was found to be 110–221˚C and 106-148˚C, respectively. The low temperature for the K/Mg geothermometer indicates a faster equilibration of K/Mg and mixing with shallow waters. The value of Na/K is not high enough for approaching equilibrium. Therefore, the reservoir temperature ought to be less than 150˚C. In addition, the Na-K-Mg diagram indicated that the temperature of geothermal water is in the range of 120-160˚C. Therefore, the reservoir temperature of the NZB ranges from 106 to 148˚C (C2), and steam loss occurs before the deep geothermal water mixing with cold water.

Along the TJF, the reservoir temperature shows change on both sides, which indicates regional fault control. The geothermal water emerges along the TJF to the surface after heating up during circulation. The circulation of geothermal water on the NE side is deeper than that on the SW side. Therefore, although both sides ascend to the surface along the TJF, different circulation depths lead to different reservoir temperatures on both sides of the TJF. The circulation depth of geothermal water of the NZB is 3.65–5.44 km, which is relatively deeper than the center area of the ZB.

Data Availability

The hydrochemical data used to support the findings of this study are included within the article.

Conflicts of Interest

The authors declare that they have no conflicts of interest.

Acknowledgments

This work was financially supported by the Basal Research Fund from the Institute of Hydrogeology and Environmental Geology, Chinese Academy of Geological Sciences (no. SK201501), the Projects of China Geological Survey (no. DD20160191), and the National Natural Science Foundation of China (nos. 41741018 and 41672249). The manuscript benefited from numerous constructive comments by X.Y. Chen and W.Z. Nian of Minnan Geological Survey Team. We also thank C.L. Liu and X.X. Yan for the support during the sample collection.

References

[1] D. X. Li and L. H. Zeng, "The study of geothermal distribution in Zhangzhou geothermal area and a preliminary model of its geothermal formation," *Earth Science*, vol. 3, pp. 229–239, 1988.

[2] Q. X. Zhuang, "Discussion on thermogenetic model of Zhangzhou geothermal field," *Earth Science*, vol. 3, pp. 335–339, 1988.

[3] V. N. Pham, D. Boyer, X. C. Yuan, and S. C. Liu, "Application of telluric-telluric profiling combined with magnetotelluric and self-potential methods to geothermal exploration in the Fujian Province, China," *Journal of Volcanology and Geothermal Research*, vol. 65, no. 3-4, pp. 227–236, 1995.

[4] Y. C. Zeng, Z. Su, N. Y. Wu, X. X. Wang, and J. Hu, "Temperature distribution characteristics of bedrock fracture groundwater system at Zhangzhou geothermal field," *Journal of Jilin University (Earth Science Edition)*, vol. 42, pp. 814–820, 2012.

[5] W. J. Lin, F. W. Wang, H. N. Gan, F. Ma, and G. L. Wang, "Site selection and development prospect of a hot dry rock resource project in Zhangzhou geothermal field, Fujian province," *Science & Technology Review*, vol. 33, pp. 28–34, 2015.

[6] Z. H. Pang, *Zhangzhou Basin geothermal system–genesis model, energy potential and the occurrence of thermal water*, Institute of Geology and Geophysics, CAS. graduation thesis, 1987.

[7] Q. Z. Han and Q. X. Zhuan, "On the source and pathway of hot water in Zhangzhou Basin, Fujian," *Earth Science*, vol. 3, pp. 271–277, 1988.

[8] J. Y. Wang, Z. H. Pang, and L. P. Xiong, "The genesisi analysis of Zhangzhou geothermal field," in *The Third China Geothermal Conference*, pp. 116–122, Shandong, China, 1989.

[9] S. B. Hu and L. P. Xiong, "Reservoir modelling of Zhangzhou low temperature fracture zone system, Fujian, China,"

Geological Science and Technology Information, vol. 4, pp. 65–71, 1990.

[10] S. B. Xiong, D. M. Jin, K. Z. Sun, Y. S. Zou, X. B. Fan, and X. G. Du, "Some characteristics of deep structure of the Zhangzhou geothermal field and its neighbourhood in Fujian Province," *Acta Geophysica Sinica*, vol. 1, pp. 55-56, 1991.

[11] W. Z. Nian, "Formation model of geothermal field and its relation with control structure in Zhangzhou," *Safety and Environmental Engineering*, vol. 4, pp. 30–33, 2008.

[12] H. N. Gan, W. J. Lin, G. F. Yue, X. Wang, F. Ma, and G. L. Wang, "Research on the fault controlling mechanism of geothermal water in Zhangzhou Basin," *Journal of Groundwater Science and Engineering*, vol. 5, pp. 326–335, 2017.

[13] X. H. Li, "Cretaceous magmatism and lithospheric extension in Southeast China," *Journal of Asian Earth Sciences*, vol. 18, no. 3, pp. 293–305, 2000.

[14] D. Wang and L. Shu, "Late Mesozoic basin and range tectonics and related magmatism in Southeast China," *Geoscience Frontiers*, vol. 3, no. 2, pp. 109–124, 2012.

[15] P. Sun, Y. Niu, P. Guo, L. Ye, J. Liu, and Y. Feng, "Elemental and Sr–Nd–Pb isotope geochemistry of the Cenozoic basalts in Southeast China: insights into their mantle sources and melting processes," *Lithos*, vol. 272-273, pp. 16–30, 2017.

[16] H. W. Zheng, R. Gao, T. D. Li, Q. S. Li, and R. Z. He, "Collisional tectonics between the Eurasian and Philippine Sea plates from tomography evidences in Southeast China," *Tectonophysics*, vol. 606, pp. 14–23, 2013.

[17] W. X. Zhu and W. S. Tu, "Curie isodepth surface of the Zhangzhou area, South Fujian," *Earth Science*, vol. 3, pp. 15–20, 1988.

[18] E. Almirudis, E. R. Santoyo-Gutierrez, M. Guevara, F. Paz-Moreno, and E. Portugal, "Chemical and isotopic signatures of hot springs from east-central Sonora State, Mexico: a new prospection survey of promissory low-to-medium temperature geothermal systems," *Revista Mexicana de Ciencias Geológicas*, vol. 35, no. 2, pp. 116–141, 2018.

[19] G. L. Long and J. D. Winefordner, "Limit of detection. A closer look at the IUPAC definition," *Analytical Chemistry*, vol. 55, no. 7, pp. 712A–724A, 1983.

[20] J. Wang, R. Zuo, and J. Caers, "Discovering geochemical patterns by factor-based cluster analysis," *Journal of Geochemical Exploration*, vol. 181, pp. 106–115, 2017.

[21] Y. H. Kao, S. W. Wang, S. K. Maji et al., "Hydrochemical, mineralogical and isotopic investigation of arsenic distribution and mobilization in the Guandu wetland of Taiwan," *Journal of Hydrology*, vol. 498, pp. 274–286, 2013.

[22] J. C. Davis, *Statistics and Data Analysis in Geology*, John Wiley & Sons, Inc., New York, NY, USA, 2nd edition, 1990.

[23] L. S. Kalkstein, G. Tan, and J. A. Skindlov, "An evaluation of three clustering procedures for use in synoptic climatological classification," *Journal of Climate and Applied Meteorology*, vol. 26, no. 6, pp. 717–730, 1987.

[24] A. H. Truesdell and R. O. Fournier, "Procedure for estimating the temperature of a hot-water component in a mixed water by using a plot of dissolved silica versus enthalpy," *Journal of Research of the U.S. Geological Survey*, vol. 5, pp. 49–52, 1977.

[25] M. Burgos, *Geothermal Interpretation of Thermal Fluid Discharge from Wells and Springs in Berlin Geothermal Field. EI Salvador, Report No. 7*, Geothermal Training Programme, Reykjavik, Iceland, 1999.

[26] Q. Guo, Z. Pang, Y. Wang, and J. Tian, "Fluid geochemistry and geothermometry applications of the Kangding high-temperature geothermal system in eastern Himalayas," *Applied Geochemistry*, vol. 81, pp. 63–75, 2017.

[27] D. E. White, "Saline waters of sedimentary rocks," in *Fluids in Subsurface Environments*, P. Young and J. E. Galley, Eds., pp. 342–365, American Association of Petroleum Geologists Memories 4, 1965.

[28] D. E. White, "Geochemistry applied to the discovery, evaluation, and exploitation of geothermal energy resources," in *Proceedings of the United Nations Symposium on the Development and Utilization of Geothermal Resources. IIRG, CNR*, pp. 58–80, Pisa, Italy, 1970.

[29] S. Arnórsson, "Chemical equilibria in icelandic geothermal systems-implications for chemical geothermometry investigations," *Geothermics*, vol. 12, no. 2-3, pp. 119–128, 1983.

[30] C.-H. Chen, "Chemical characteristics of thermal waters in the central range of Taiwan, R.O.C," *Chemical Geology*, vol. 49, no. 1-3, pp. 303–317, 1985.

[31] C. W. Karingithi, "Chemical geothermometers for geothermal exploration," in *Short Course IV on Exploration for Geothermal Resources*, pp. 1–22, United Nations University, Geothermal Training Program, Lake Vaivasha, Kenya, 2009.

[32] C. M. Liu, H. T. Chiang, C. H. Kuo, S. R. Song, and Y. W. Tsai, "Integrating geothermometer and high resolution thermometer to characterize the geothermal characteristics of Ilan Plain, Taiwan," in *40th Workshop on Geothermal Reservoir Engineering*, pp. 1–6, Stanford University, Stanford, California, 2015.

[33] Y. H. Huang, H. L. Liu, S. R. Song, and H. F. Chen, "An ideal geothermometer in slate formation: a case from the Chingshui geothermal field, Taiwan," *Geothermics*, vol. 74, pp. 319–326, 2018.

[34] R. O. Fournier and W. L. Marshall, "Calculation of amorphous silica solubilities at 25° to 300°C and apparent cation hydration numbers in aqueous salt solutions using the concept of effective density of water," *Geochimica et Cosmochimica Acta*, vol. 47, no. 3, pp. 587–596, 1983.

[35] R. O. Fournier and J. J. Rowe, "Solubility of amorphous silica in water at high temperatures and high-pressures," *American Mineralogist*, vol. 62, pp. 1052–1056, 1977.

[36] A. J. Ellis and S. H. Wilson, "The geochemistry of alkali metal ions in the Wairakei hydrothermal system," *New Zealand Journal of Geology and Geophysics*, vol. 3, no. 4, pp. 593–617, 1960.

[37] A. J. Ellis and W. A. J. Mahon, "Natural hydrothermal systems and experimental hotwater/rock interactions," *Geochimica et Cosmochimica Acta*, vol. 28, no. 8, pp. 1323–1357, 1964.

[38] R. O. Fournier, "Geochemical and hydrologic considerations and the use of enthalpy-chloride diagrams in the prediction of underground conditions in hot-spring systems," *Journal of Volcanology and Geothermal Research*, vol. 5, no. 1-2, pp. 1–16, 1979.

[39] Q. Guo, Y. Wang, and W. Liu, "Hydrogeochemistry and environmental impact of geothermal waters from Yangyi of Tibet, China," *Journal of Volcanology and Geothermal Research*, vol. 180, no. 1, pp. 9–20, 2009.

[40] X. Wang, G. Wang, C. Lu, H. Gan, and Z. Liu, "Evolution of deep parent fluids of geothermal fields in the Nimu-Nagchu geothermal belt, Tibet, China," *Geothermics*, vol. 71, pp. 118–131, 2018.

[41] R. O. Fournier, "Chemical geothermometers and mixing models for geothermal systems," *Geothermics*, vol. 5, no. 1-4, pp. 41–50, 1977.

[42] S. P. Verma and E. Santoyo, "New improved equations for NaK, NaLi and SiO_2 geothermometers by outlier detection and rejection," *Journal of Volcanology and Geothermal Research*, vol. 79, no. 1-2, pp. 9–23, 1997.

[43] R. O. Fournier, "Application of water geochemistry to geothermal exploration and reservoir engineering," in *Geothermal Systems: Principles and Case Histories*, L. Rybach and L. J. P. Muffler, Eds., pp. 109–143, John Wiley and Sons Ltd., New York, NY, USA, 1981.

[44] W. F. Giggenbach, "Geothermal solute equilibria. Derivation of Na-K-Mg-Ca geoindicators," *Geochimica et Cosmochimica Acta*, vol. 52, no. 12, pp. 2749–2765, 1988.

[45] F. Nitschke, S. Held, T. Neumann, and T. Kohl, "Geochemical characterization of the Villarrica geothermal system, Southern Chile, part II: site-specific re-evaluation of SiO_2, and Na-K solute geothermometers," *Geothermics*, vol. 74, pp. 217–225, 2018.

[46] S. Arnórsson, S. Sigurdsson, and H. Svavarsson, "The chemistry of geothermal waters in Iceland. I. Calculation of aqueous speciation from 0° to 370°C," *Geochimica et Cosmochimica Acta*, vol. 46, no. 9, pp. 1513–1532, 1982.

[47] S. Arnórsson, *Isotopic and Chemical Techniques in Geothermal Exploration, Development and Use*, International Atomic Energy Agency, Vienna, 2000.

[48] B. Q. Zhu, L. X. Zhu, C. Y. Shi, and H. Yu, *Geochemical Exploration of Geothermal Fields*, Geological Publishing House, Beijing, 1992.

[49] X. Wang, G. L. Wang, H. N. Gan, Z. Liu, and D. W. Nan, "Hydrochemical characteristics and evolution of geothermal fluids in the Chabu high-temperature geothermal system, Southern Tibet," *Geofluids*, vol. 2018, Article ID 8532840, 15 pages, 2018.

[50] W. Wagner and H. J. Kretzschmar, *International Steam Tables, Properties of Water and Steam Based on the Industrial Formulation IAPWS-IF97, second edition*, Springer-Verlag, Berlin, 2008.

[51] Z. H. Pang, Z. C. Fan, and J. Y. Wang, "The study on stable oxygen and hydrogen isotopes in the Zhangzhou Basin hydrothermal system," *Acta Petrologica Sinica*, vol. 4, pp. 75–84, 1990.

[52] Minnan Geological Survey Team, *Report of Detailed Survey in Zhangzhou Geothermal Field (in Chinese)*, Minnan Geological Survey Team Press, Zhangzhou, China, 2007.

[53] L. P. Xiong, J. Y. Wang, and Z. H. Pang, "Convective and conductive heat flows in Zhangzhou geothermal field, Fujian Province, China," *Acta Geophysica Sinica*, vol. 6, pp. 702–711, 1990.

[54] L. P. Xiong, J. Y. Wang, and Z. H. Pang, "Circulation depth of the thermal water in Zhangzhou geothermal field," *Chinese Journal of Geology*, vol. 4, pp. 377–384, 1990.

[55] G. Wang, W. Lin, W. Zhang, C. Lu, F. Ma, and H. Gan, "Research on formation mechanisms of hot dry rock resources in China," *Acta Geologica Sinica*, vol. 90, no. 4, pp. 1418–1433, 2016.

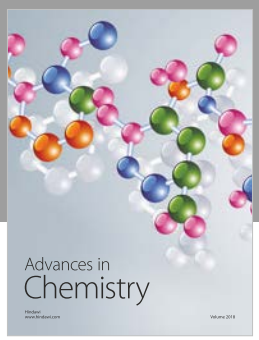

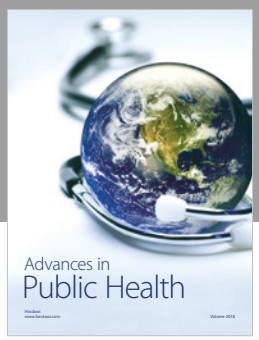

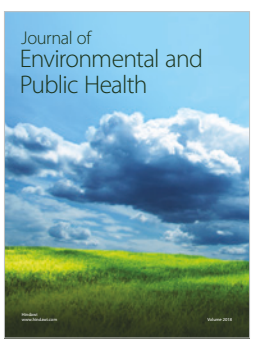

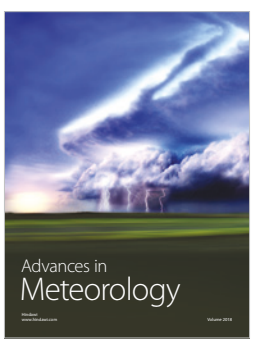

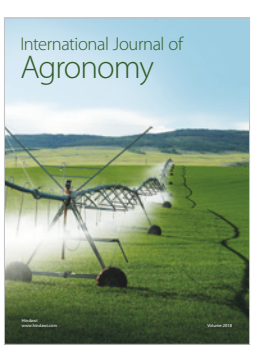

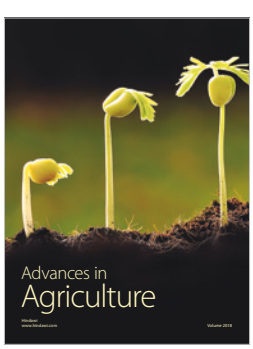

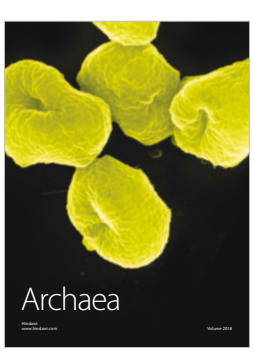

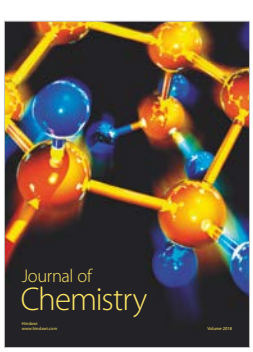


Hindawi

Submit your manuscripts at
www.hindawi.com